INTERNATIONAL JOURNAL FOR NUMERICAL METHODS IN FLUIDS
Int. J. Numer. Meth. Fluids 2009; **59**:753–765
Published online 9 July 2008 in Wiley InterScience (www.interscience.wiley.com). DOI: 10.1002/fld.1836

Numerical modeling of turbulent compound channel flow using the lattice Boltzmann method

H. Liu*, †, J. G. Zhou and R. Burrows

Department of Engineering, University of Liverpool, Liverpool L69 3GQ, U.K.

SUMMARY

The flow of water in a straight compound channel with prismatic cross section is investigated with a relatively new tool, the lattice Boltzmann method. The large eddy simulation model is added in the lattice Boltzmann model for nonlinear shallow water equations (LABSWE^{TM}) so that the turbulence, caused by lateral exchange of momentum in the shear layer between the main channel and floodplain, can be taken into account and modeled efficiently. To validate the numerical model, a symmetrical compound channel with trapezoidal main channel and flat floodplain is tested. Similar to most natural watercourses, the floodplain has higher roughness values than the main channel. Different relative depths, D_r (the ratio of the depth of flow on the floodplain to that in the main channel), are considered. The Reynolds number is set at 30 000 in the main channel. The lateral distributions of the longitudinal velocity, the boundary shear stress, the Reynolds stress and the apparent shear stress across the channel are obtained after the large eddy simulation is performed. The results of numerical simulations are compared with the available experiment data, which show that the LABSWE^{TM} is capable of modeling the features of flow turbulence in compound channels and is sufficiently accurate for practical applications in engineering. Copyright © 2008 John Wiley & Sons, Ltd.

Received 17 December 2007; Revised 31 March 2008; Accepted 1 April 2008

KEY WORDS: compound channel flow; lattice Boltzmann method; large eddy simulation; boundary shear stress; apparent shear stress; Reynolds stress; LABSWE^{TM}

1. INTRODUCTION

Compound channel flow is of considerable importance in both practice and theory. In natural rivers, such flows happen during floods when the water level exceeds the bank elevation and occupies the adjacent floodplain. Also certain man-made compound channels are deliberately constructed to increase the conveyance capacity during flooding or to provide additional recreational space for

*Correspondence to: H. Liu, Department of Engineering, University of Liverpool, Liverpool L69 3GQ, U.K.
†E-mail: Haifei.Liu@liv.ac.uk

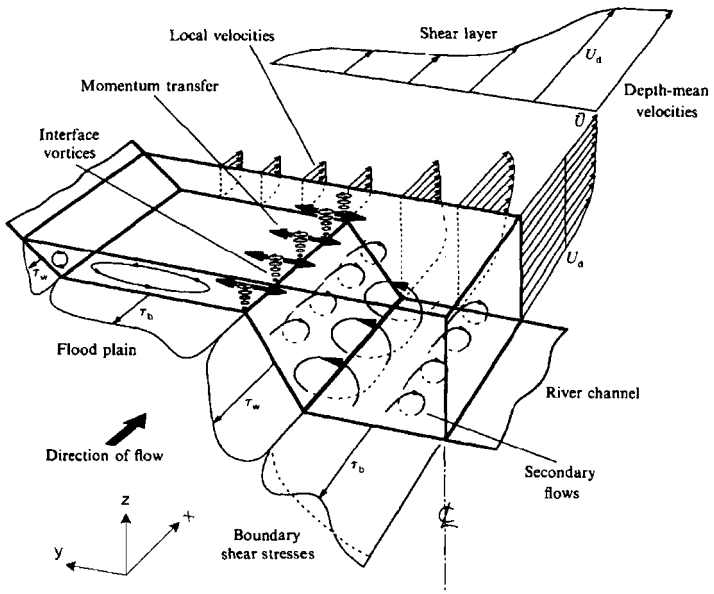

Figure 1. Features of flows in two-stage compound channel [9].

sightseeing, etc. [1]. As many engineering projects aim at flood mitigation, the prediction of flow characteristics in compound channels is of much concern. The traditional approach to compound channel flow is conceptually to divide the flow into subsections and compute separately [2], without considering the interaction between the main channel and the floodplain. In reality, an exchange of momentum exists, as pointed out by Wright and Carstens [3], and by Zheleznyakov [3, 4]. A large number of experiments were carried out in the 1980s. Contributions from Hadjipanos [5], Wormleaton *et al.* [6], Knight and Demetriou [7], Myers [8] and other researchers provided abundant data leading to a better understanding of the fundamental behavior of compound channel flow. Representative features of flows in a two-stage symmetric compound channel are sketched in Figure 1. Subsequently, several analytical models have been developed by involving empirical coefficients, assumptions or approximations [10–12]. With the development of computing power, numerical simulation has become one of the main means to investigate fluid problems and is now popular in both academia and industry. For example, Rameshwaran and Naden [13] and Morvan *et al.* [14] simulated compound channel flows using conventional three-dimensional models. However, these three-dimensional models require huge computational capacity, whereas one-dimensional models are clearly not sufficient for this purpose. Thus, two-dimensional models based on depth-averaged parameters are suitable, especially for the lateral distribution of velocity and shear stress. An alternative tool, the lattice Boltzmann model for nonlinear shallow water equations (LABSWE^{TM}), has been developed and improved theoretically over the past decade [15]. Since the flow characteristics in a compound channel is strongly dependent on local source terms, and the lattice Boltzmann method (LBM), based on micro-dynamics, is able to model macroscopic phenomena without loss of detailed features, the two-dimensional LABSWE^{TM} [15] is considered here to investigate compound channel flows. The aim of this paper is to examine the capacity of the lattice Boltzmann model to predict compound channel flow.

DOI: 10.1002/fld

In straight channel flow, turbulence is generated by boundary shear, the velocity gradient, and the secondary flow of Prandtl's second type. The standard subgrid-scale stress model is here incorporated into the LBM for nonlinear shallow water equations (LABSWE^{TM}) so that turbulence can be taken into account and modeled efficiently, especially so as to treat the turbulence caused by lateral exchange of momentum in the shear layer between the main channel and floodplain. On account of symmetry of the selected straight compound channel, only half the channel model is set up. This has been verified by the data from Science and Engineering Research Council Flood Channel Facility (SERC-FCF) [9] at the University of Birmingham and by the experience from other investigations [11, 16]. In the present study, the Reynolds number of the flow is selected as 30 000 in the main channel, with reference to the SERC-FCF experimental conditions. The lateral distribution of the longitudinal velocity, the boundary shear stress, the Reynolds stress and the apparent shear stress across the channel are obtained from the numerical simulations and are then compared with the available experimental data.

2. LABSWE^{TM}

2.1. Governing equations

Water depth in shallow water flow is usually much smaller than horizontal scale so that flow is characterized by horizontal motion. The assumption of hydrostatic pressure is often used to replace the momentum equation in the vertical direction in the mathematical model; therefore, the vertical acceleration is ignored. On the other hand, most flows in nature are turbulent. In theory, turbulence can be simulated using the Navier–Stokes equations and the continuity equation, but at enormous computational overhead. Generally, there are two alternative ways to model turbulence: introducing the Reynolds equations and turbulent stress as in the $k-\varepsilon$ model or using space-filtered governing equations and large eddy simulation with subgrid-scale stress model for the unresolved scale stress. Previous research indicates that the latter approach produces more accurate solutions and gives very detailed turbulent features [17]; hence it is used in this paper. The general two-dimensional governing equations for shallow water flows can be derived from the Navier–Stokes equations. After taking depth-averaged and space-filtered calculations, the nonlinear shallow water equations can be expressed in a tensor form as [18]

$$\frac{\partial h}{\partial t}+\frac{\partial (hu_j)}{\partial x_j}=0 \tag{1}$$

$$\frac{\partial (hu_i)}{\partial t}+\frac{\partial (hu_iu_j)}{\partial x_j}=-\frac{g}{2}\frac{\partial h^2}{\partial x_i}+(\nu+\nu_e)\frac{\partial^2 (hu_i)}{\partial x_j \partial x_j}+F_i \tag{2}$$

where the Cartesian coordinate system is used; h is water depth; x_j and u_j are the distance and instantaneous space-filtered velocity components in the j direction, respectively, i.e. for $j=1$, $x_j=x$ and $u_j=u$; for $j=2$, $x_j=y$ and $u_j=v$. x and y are defined as longitudinal and lateral directions of the channel; and u_j is defined by

$$u_j(x,y,z,t)=\int\int\int_{\Delta x\Delta y\Delta z} u_j^{\mathrm{b}} G(x,y,z,x',y',z')\,\mathrm{d}x'\mathrm{d}y'\mathrm{d}z' \tag{3}$$

DOI: 10.1002/fld

with a spatial filter function G and u_j^{b} is the velocity component before being space-filtered; x', y' and z' are the coordinates of the space chosen for velocity filter; $g=9.81\,\mathrm{m/s^2}$ is the gravitational acceleration; t is the time; v is the kinematic viscosity; v_{e} is the eddy viscosity, defined by

$$v_{\mathrm{e}}=(C_{\mathrm{s}}l_{\mathrm{s}})^2\sqrt{S_{ij}S_{ij}} \tag{4}$$

where C_{s} is the Smagorinsky constant, $l_{\mathrm{s}}=\Delta x$ and S_{ij} is the magnitude of the large-scale strain-rate tensor:

$$S_{ij}=\frac{1}{2h}\left[\frac{\partial(hu_i)}{\partial x_j}+\frac{\partial(hu_j)}{\partial x_i}\right] \tag{5}$$

The depth-averaged subgrid-scale stress τ_{ij} with eddy viscosity is calculated by

$$\tau_{ij}=-v_{\mathrm{e}}\left[\frac{\partial(hu_i)}{\partial x_j}+\frac{\partial(hu_j)}{\partial x_i}\right] \tag{6}$$

In addition, F_i is the force term and is defined as

$$F_i=-gh\frac{\partial z_b}{\partial x_i}+\frac{\tau_{wi}-\tau_{bi}}{\rho} \tag{7}$$

where z_b is the bed elevation above the datum. The bed shear stress τ_{bi} in the i direction is given by the depth-averaged velocities:

$$\tau_{bi}=\rho C_b u_i\sqrt{u_j u_j} \tag{8}$$

in which C_b is the bed friction coefficient estimated from $C_b=g/C_z^2$. C_z is the Chezy coefficient either given by the Manning equation, $C_z=h^{1/6}/n_b$, where n_b is the Manning coefficient, or the Colebrook–White equation [19]:

$$C_z=-\sqrt{32g}\lg\left(\frac{K_{\mathrm{s}}}{14.8h}+\frac{1.255vC_z}{4h\sqrt{2gu_ju_j}}\right) \tag{9}$$

where K_{s} is the Nikuradse equivalent sand roughness. The wind shear stress $\tau_{wi}=\rho_{\mathrm{a}}C_w u_{wi}\sqrt{u_{wj}u_{wj}}$ where ρ_{a} is the density of air, C_w is the resistance coefficient and u_{wi} is the component of the wind velocity in the i direction.

2.2. *Lattice Boltzmann model*

The LBM is a discrete computational method based on lattice gas cellular automata. A lattice Boltzmann model has three main components: the kinetic equation; a lattice pattern and the equilibrium distributions. The lattice Boltzmann model for nonlinear shallow water equations (LABSWE) has been presented by Zhou [15]. After incorporating the subgrid-scale model, for motion in the i direction the lattice Boltzmann equation with 9-speed square lattice and force term is given as follows:

$$f_\alpha(x+e_\alpha\Delta t,t+\Delta t)=f_\alpha(x,t)-\frac{1}{\tau_{\mathrm{t}}}[f_\alpha(x,t)-f_\alpha^{\mathrm{eq}}(x,t)]+\frac{\Delta t}{6e^2}e_{\alpha i}F_i \tag{10}$$

where f_α is the particle distribution function; $e=\Delta x/\Delta t$; Δx is the lattice size; Δt is the time step; $\tau_{\mathrm{t}}=\tau+\tau_{\mathrm{e}}$ is the total relaxation time, wherein τ is the single relaxation time and τ_{e} is the eddy

DOI: 10.1002/fld

relaxation time with respect to the eddy viscosity. Since τ_e can be calculated by

$$\tau_e = \frac{-\tau + \sqrt{\tau^2 + 18C_s^2/(e^2 h)\sqrt{\prod_{ij}\prod_{ij}}}}{2} \tag{11}$$

the total relaxation time, τ_t, is further expressed as

$$\tau_t = \frac{\tau + \sqrt{\tau^2 + 18C_s^2/(e^2 h)\sqrt{\prod_{ij}\prod_{ij}}}}{2} \tag{12}$$

where

$$\prod_{ij} = \sum_{\alpha} e_{\alpha i} e_{\alpha j} (f_\alpha - f_\alpha^{eq}) \tag{13}$$

$e_{\alpha i}$ is the i directional component of velocity vector of a particle in the α link. For the 9-speed square lattice shown in Figure 2(a), each particle moves one lattice unit at its velocity along one of the eight links indicated with number 1–8, or else 0 indicates the particle at rest with zero speed. The velocity vector of particles is defined by

$$e_\alpha = \begin{cases} (0,0), & \alpha = 0 \\ e\left[\cos\dfrac{(\alpha-1)\pi}{4}, \sin\dfrac{(\alpha-1)\pi}{4}\right], & \alpha = 1,3,5,7 \\ \sqrt{2}e\left[\cos\dfrac{(\alpha-1)\pi}{4}, \sin\dfrac{(\alpha-1)\pi}{4}\right], & \alpha = 2,4,6,8 \end{cases} \tag{14}$$

The local equilibrium distribution function is expressed as

$$f_\alpha^{eq} = \begin{cases} h - \dfrac{5gh^2}{6e^2} - \dfrac{2h}{3e^2}u_i u_i, & \alpha = 0 \\ \dfrac{gh^2}{6e^2} + \dfrac{h}{3e^2}e_{\alpha i}u_i + \dfrac{h}{2e^4}e_{\alpha i}e_{\alpha j}u_i u_j - \dfrac{h}{6e^2}u_i u_i, & \alpha = 1,3,5,7 \\ \dfrac{gh^2}{24e^2} + \dfrac{h}{12e^2}e_{\alpha i}u_i + \dfrac{h}{8e^4}e_{\alpha i}e_{\alpha j}u_i u_j - \dfrac{h}{24e^2}u_i u_i, & \alpha = 2,4,6,8 \end{cases} \tag{15}$$

From the distribution function, the water depth h and flow velocity u_i can be calculated from

$$h = \sum_\alpha f_\alpha, \quad u_i = \frac{1}{h}\sum_\alpha e_{\alpha i} f_\alpha \tag{16}$$

2.3. Boundary conditions

Boundary conditions play a crucial role since they select solutions that are compatible with external constraints [20]. The lattice Boltzmann equation can be solved with proper boundary conditions, such as the bounce-back scheme of no-slip boundary conditions for highly rough boundaries (see Figure 2(b)) [21]. At the inflow and outflow boundaries, it has been tested that the periodic

DOI: 10.1002/fld

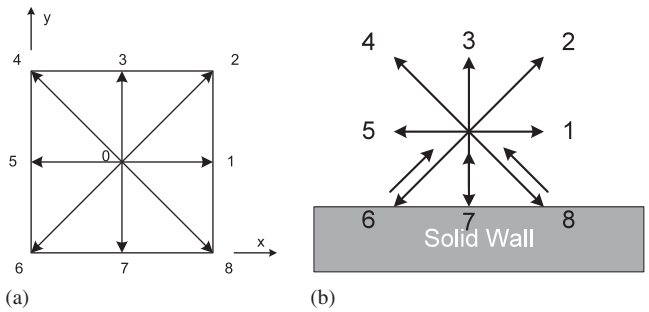

Figure 2. (a) D2Q9 and (b) bounce-back scheme.

boundary condition shows an excellent stability [22]; hence it is used in this paper. If the velocities and the depth are known, the unknown distribution function f_α at the boundaries can be calculated with the method given by Zou and He [23]. Assume $v=0$, for inflow boundary:

$$\begin{cases} f_1 = f_5 + \dfrac{2hu}{3e} \\ f_2 = \dfrac{hu}{6e} + f_6 + \dfrac{f_7 - f_3}{2} \\ f_8 = \dfrac{hu}{6e} + f_4 + \dfrac{f_3 - f_7}{2} \end{cases} \tag{17}$$

for outflow boundary:

$$\begin{cases} f_5 = f_1 - \dfrac{2hu}{3e} \\ f_4 = -\dfrac{hu}{6e} + f_8 + \dfrac{f_7 - f_3}{2} \\ f_6 = -\dfrac{hu}{6e} + f_2 + \dfrac{f_3 - f_7}{2} \end{cases} \tag{18}$$

3. NUMERICAL SIMULATION AND VALIDATION

3.1. Model dimensions and parameters

For reasons of symmetry, only half of the channel is investigated (see Figure 3), saving 50% of computation time. The dimensions of the channel are consistent with the SERC-FCF Series 02 [11]. The geometrical parameters are $B/b=4.2$, $b/H_c=5$, side slope $s=1$, $b=0.75\,\text{m}$, $H_c=0.15\,\text{m}$, bed slope $S_0=0.001$, and the bed friction factors (C_b) are 0.0163, 0.0204 and 0.0245 for zones 1–3, respectively. H is controlled between 0.2 and 0.3 m giving D_r ($=(H-H_c)/H$) between 0.15 and 0.4 (H_c is the depth of the main channel). The computational domain is $10\,\text{m}\times 3.15\,\text{m}$ with a 200×64 grid. $\tau=0.5001$ and time step $\Delta t=0.001\,\text{s}$. A periodic boundary condition is applied at the inflow and outflow boundaries, whereas a no-slip boundary condition is used at the rough bank side.

DOI: 10.1002/fld

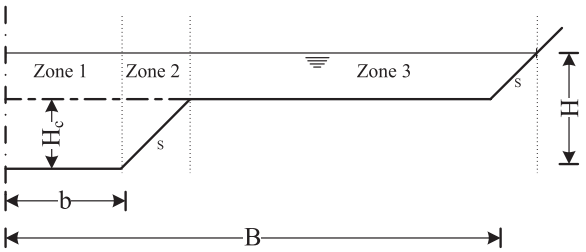

Figure 3. Compound channel sketch.

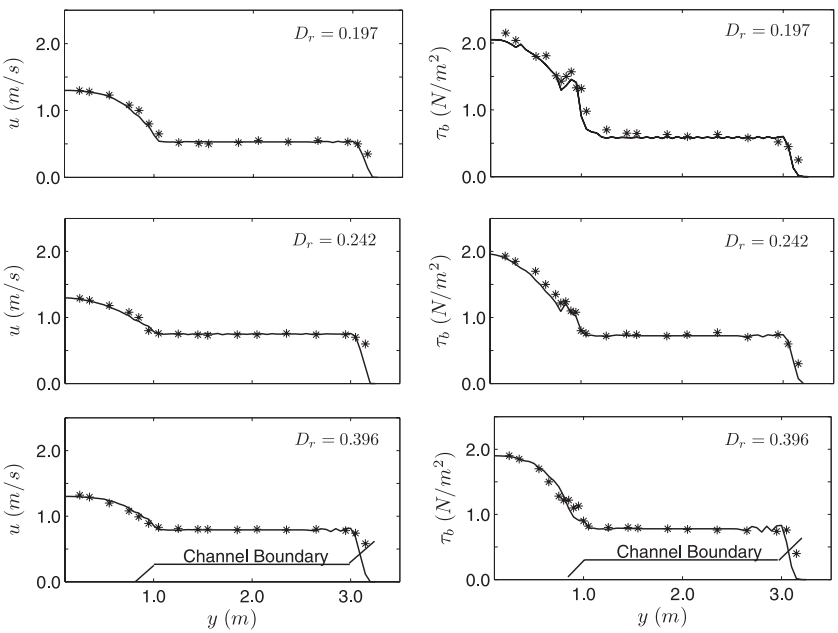

Figure 4. Comparison between the LBM (—) and the FCF experimental ($*$) lateral distributions of u and τ_b.

3.2. Velocity and boundary shear stress

The results for longitudinal velocity and boundary shear stress shown in Figure 4 indicate that the LBM predictions give overall agreement with the FCF data, although the LBM results underestimate both u and τ_b (Equation (8)) slightly in the main channel when D_{r} is small. However, the situation is better as the value of D_{r} increases. It should be noted that the deviations near the bank are relatively higher than the other areas, which is probably caused by the application of the no-slip boundary condition, assuming that the boundaries are highly rough. This can be improved by using the semi-slip boundary condition [21]. The curves of boundary shear stress τ_b show sudden increase adjacent to the transitional area where the bed friction is discontinuous, but the jumps of τ_b become less noticeable with the ascending of D_{r}.

DOI: 10.1002/fld

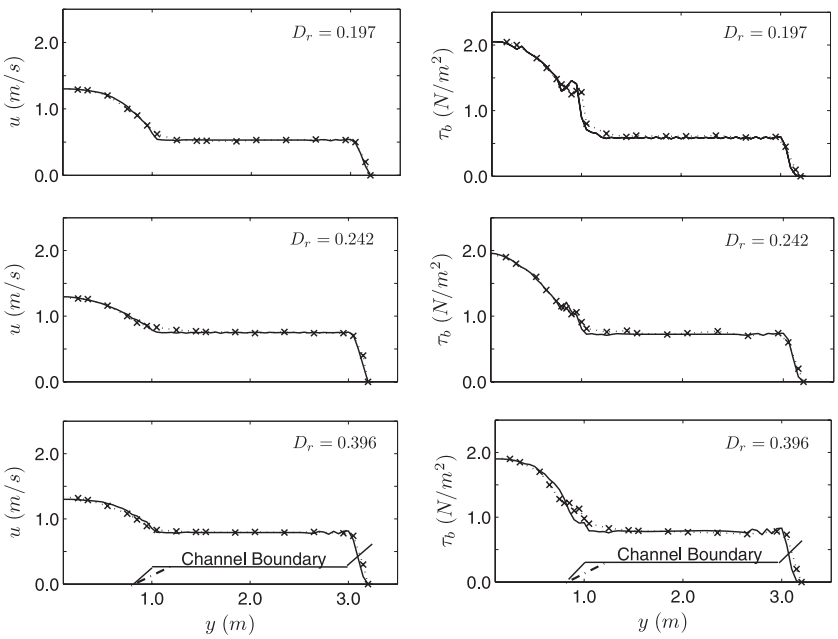

Figure 5. Comparison between the LBM lateral distributions of u and τ_b with different side slopes: $s=1$ (—) and $s=0.577$ (×).

Additionally, as most natural channels have side slopes smaller than 1 (45°), another side slope $s=0.577$ (30°) is investigated with the other conditions remaining the same as for the previous test. As shown in Figure 5, the change of the side slope does not influence the lateral distributions of longitudinal velocity and boundary shear stress significantly for any value of D_{r} involved in this study. However, the shear effect is slightly weakened giving rise to the smoother curves, although the shear layer is a bit larger than that for $s=1$.

3.3. The Reynolds stress

The velocity histories, representing the instantaneous velocities with perturbation around the mean values at two typical points across the channel, are plotted in Figure 6. The coordinates of these two points are (2.00 m, 0.25 m) in the main channel and (2.00 m, 0.85 m) in the shear layer. In fact, such mean velocities are constants for dynamic steady flows. The turbulence modeling based on a subgrid-scale stress model gives detailed fluctuation of velocities, which represents one of the advantages over time-averaged turbulence models such as the $k-\varepsilon$ model.

The Reynolds stress can be obtained by the definition $\tau_{xy}^{\mathrm{R}} = -\rho\overline{u'v'}$, where u' and v' are turbulent perturbations of velocity and calculated by

$$u' = u - \bar{u}, \quad v' = v - \bar{v} \tag{19}$$

where $\bar{u}$ and $\bar{v}$ are time-averaged velocities. Because the turbulence is significant in the shear layer due to the lateral exchange of momentum, the distribution of the Reynolds stresses in and near the shear layer is of interest and is plotted in Figure 7. The figure shows good agreement between the

DOI: 10.1002/fld

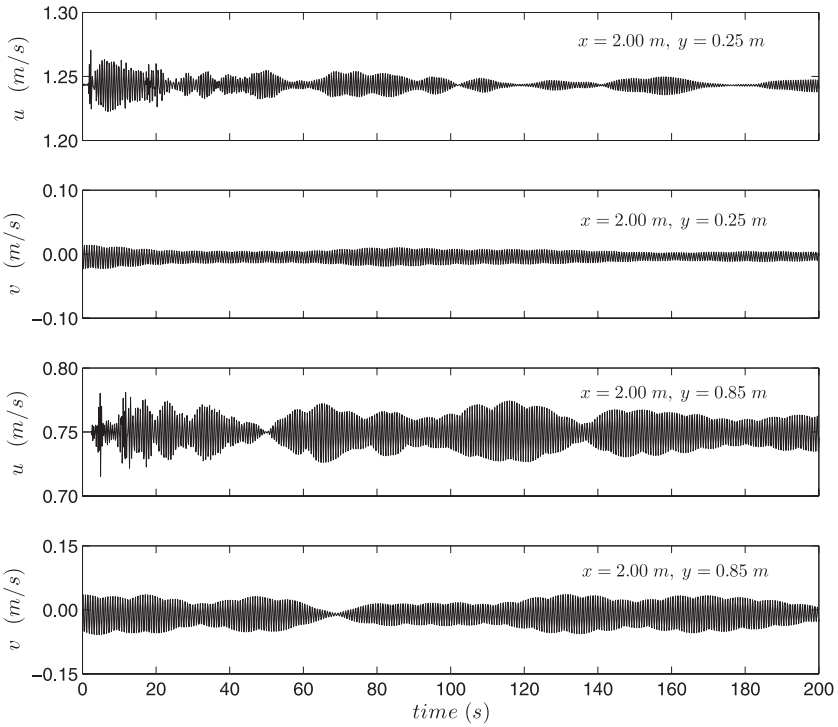

Figure 6. Typical velocity history in turbulent compound channel flow ($D_r = 0.242$).

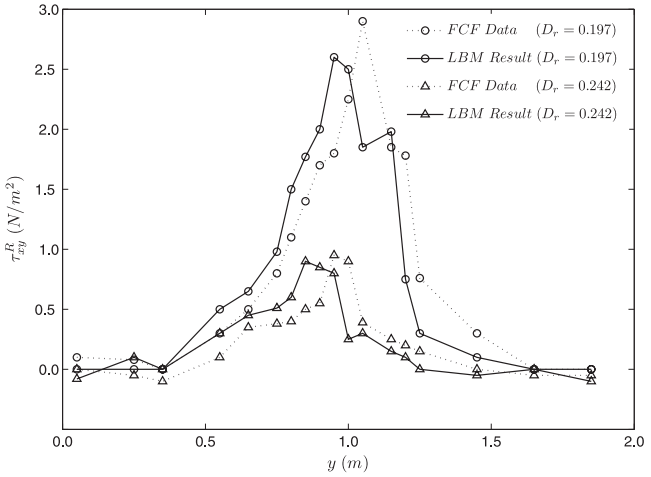

Figure 7. The Reynolds stress τ_{xy}^{R} near shear layer.

DOI: 10.1002/fld

LBM results and the FCF data with the maximum difference taking place at the interface between the main channel and floodplain ($y=0.9$ m). This may be caused by the complex three-dimensional flow structure due to the strong effect of the secondary flow in this region. For D_r values above 0.197, the peak of τ_{xy}^R decreases by about 60%, indicating that the turbulence is less distinct.

3.4. Apparent stress

The depth-mean apparent shear stress acting on a vertical interface τ_{xy}^A may be calculated by the coupling of the Newtonian shear stress model and the subgrid-scale stress model:

$$\tau_{xy}^A = \mu \frac{\partial h u_i}{\partial x_j} - \nu_e \left[\frac{\partial (h u_i)}{\partial x_j} + \frac{\partial (h u_j)}{\partial x_i} \right] \tag{20}$$

The eddy viscosity ν_e may be calculated by Equation (4). It should be noted that the velocity used here is still instantaneous and space-filtered. To verify the model, the LBM result is compared with the experimental data for $D_r=0.197$, shown in Figure 8. The agreement between the two curves indicates the applicability of the lattice Boltzmann model.

Subsequently, the model is applied to another two cases of D_r, 0.242 and 0.396, respectively. As can be seen from Figure 9, generally the smaller D_r gives the larger absolute value of τ_{xy}^A across the channel, especially adjacent to the interface of the main channel and the floodplain. However, the peak value occurs within the floodplain immediately adjacent to the interface. Also, with decrease in D_r, the peak of the curves moves to the right gradually showing that the influence of momentum exchange transfers further into the floodplain. In addition, τ_{xy}^A varies approximately linearly in both the main channel and the floodplain, which is consistent with the first-order assumption of the analytical solution proposed by Shiono and Knight [24].

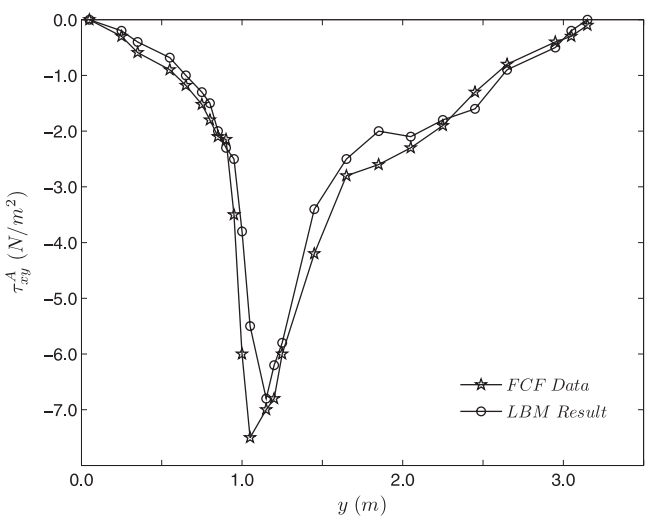

Figure 8. Comparison between the LBM and the FCF experimental apparent shear stresses τ_{xy}^A for $D_r=0.197$.

DOI: 10.1002/fld

4. SUMMARY AND DISCUSSION

This paper describes the LBM for nonlinear shallow water equations coupled with the large eddy simulation model (LABSWE^{TM}) and its application to compound channel flows. Numerical simulations have been carried out for different relative depths (D_r), and the lateral distributions of longitudinal velocity, boundary shear stress, Reynolds stress and apparent shear stress have been analyzed. The normalized root-mean-square error and the maximum error have been calculated and shown in Table I, indicating that good agreement has been achieved. In terms of run time, generally, a two-dimensional model uses much shorter time and less storage than a three-dimensional model. Although there is no literature stating the run time for the three-dimensional compound channel modeling, from previous research [25, 26], the lattice Boltzmann model used even shorter time than a conventional model for the same dimensional task; on the other hand, since the distribution

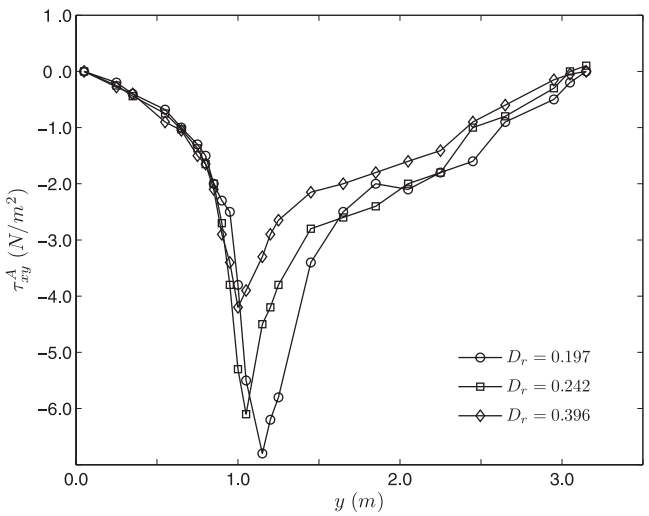

Figure 9. The LBM apparent shear stress τ_{xy}^{A} comparison for different D_r.

Table I. Normalized Rms-error and max-error.

	D_r	Rms-error*	Max-error*
u	0.197	0.048	0.271
	0.242	0.037	0.255
	0.396	0.024	0.323
τ_b	0.197	0.033	0.178
	0.242	0.029	0.125
	0.396	0.028	0.211
τ_{xy}^{R}	0.197	0.155	0.379
	0.242	0.235	0.421
τ_{xy}^{A}	0.197	0.092	0.440

Rms: root-mean-square.
*Normalized by the maximum experimental data.

DOI: 10.1002/fld

function, f, is the only variable in the LBM, the requirement of storage is lower than a traditional model, which also gives rise to an increase in the running speed.

5. CONCLUSIONS

The numerical simulations confirm the ability of the lattice Boltzmann model to simulate accurately compound channel flow. In practice, secondary flow generated by the channel geometry makes the flow structure three-dimensional in the vicinity of the shear layers. The present numerical results (obtained by reducing the problem to a two-dimensional depth-averaged case) demonstrate that the model achieves acceptable accuracy while requiring considerably less computing power than conventional three-dimensional simulations.

REFERENCES

1. Knight DW, Shamseldin AY. *River Basin Modelling for Flood Risk Mitigation*. Taylor & Francis Group: London, Philadelphia, PA, 2005.
2. Chow VT. *Open Channel Hydraulics*. McGraw-Hill: New York, 1959.
3. Wright PR, Carstens HR. Linear momentum flux to overbank sections. *Journal of the Hydraulics Division* (ASCE) 1970; **96**(9):1781–1793.
4. Zheleznyakov GV. Interaction of channel and flood plain streams. *Proceedings of 14th IAHR Congress*, Paris, France, 1971; 144–148.
5. Hadjipanos P. Flow in compound channels with varying roughness. *Thesis*, University of London, 1980.
6. Wormleaton PR, Allen J, Hadjipanos P. Discharge assessment in compound channel flow. *Journal of the Hydraulics Division* (ASCE) 1982; **108**(9):975–993.
7. Knight DA, Demetriou JD. Floodplain and main channel flow interaction. *Journal of Hydraulic Engineering* (ASCE) 1983; **110**(10):1412–1430.
8. Myers WRC. Velocity and discharge in compound channels. *Journal of Hydraulic Engineering* (ASCE) 1987; **113**(6).
9. Shiono K, Knight DW. Turbulent open-channel flows with variable depth across the channel. *Journal of Fluid Mechanics* 1991; **222**:617–646.
10. van Prooijen BC, Battjes JA, Uijttewaal WSJ. Momentum exchange in straight uniform compound channel flow. *Journal of Hydraulic Engineering* 2005; **131**:175–183.
11. Knight DW, Shiono K. Turbulence measurements in a shear layer region of a compound channel. *Journal of Hydraulic Research* 1990; **28**:175–196.
12. Ervine DA, Babaeyan-Koopaei K, Sellin RHJ. Two-dimensional solution for straight and meandering overbank flows. *Journal of Hydraulic Engineering* 2000; **126**:653–669.
13. Rameshwaran P, Naden PS. Three-dimensional numerical simulation of compound channel flows. *Journal of Hydraulic Engineering* 2003; **129**:645–652.
14. Morvan H, Pender G, Wright NG, Ervine DA. Three-dimensional hydrodynamics of meandering compound channels. *Journal of Hydraulic Engineering* 2002; **128**(8):674–682.
15. Zhou JG. A lattice Boltzmann model for the shallow water equations with turbulence modeling. *International Journal of Modern Physics C* 2002; **13**(8):1135–1150.
16. Patel VC. Calibration of the Preston tube and limitations on its use in pressure gradients. *Journal of Fluid Mechanics* 1965; **23**:185–195.
17. Tutar M, Hold AE. Computational modelling of flow around a circular cylinder in sub-critical flow regime with various turbulence models. *International Journal for Numerical Methods in Fluids* 2001; **35**:763–784.
18. Zhou JG. *Lattice Boltzmann Methods for Shallow Water Flows*, vol. 1. Springer: Berlin, Germany, 2004.
19. Featherstone RE, Nalluri C. *Civil Engineering Hydraulics* (3rd edn). Hartnolls Ltd: Bodmin, Cornwall, Great Britain, 1995.
20. Succi S. *The Lattice Boltzmann Equation for Fluid Dynamics and Beyond*. Oxford University Press: Oxford, 2001.

DOI: 10.1002/fld

21. Zhou JG. An elastic-collision scheme for lattice Boltzmann methods. *International Journal of Modern Physics C* 2001; **12**:387–401.
22. Sukop MC, Thorne DT. *Lattice Boltzmann Modeling—An Introduction for Geoscientists and Engineers*. Springer: New York, 2006.
23. Zou Q, He X. On pressure and velocity boundary conditions for the lattice Boltzmann BGK model. *Physics of Fluids* 1997; **9**:1591–1598.
24. Shiono K, Knight DW. Two dimensional analytical solution for a compound channel. *Proceedings of 3rd International Symposium on Refined Flow Modeling and Turbulence Measurements*, Tokyo, Japan, 1988; 503–510.
25. Liu Y, So RMC, Cui ZX. Bluff body flow simulation using lattice Boltzmann equation with multiple relaxation time. *Computers and Fluids* 2005; **35**:951–956.
26. Liu H, Zhou JG, Burrows R. Bridge afflux predictions using the lattice Boltzmann method. *Journal of Fluids and Structures* 2008; submitted.

DOI: 10.1002/fld